High resolution imaging of non-equilibrium colloidal self-assembly enabled by photopolymerization

Author List: *Jagannath Satpathy[a], Jim Jui-Kai Chen[a], Gang Wen[a],[b], Hiroshi Masuhara[c], Sudipta Seth[a], Volker Leen[e], Susana Rocha[a], Johan Hofkens*[a],[f], Boris Louis*[a], Roger Bresolí-Obach*[a],[d]*

Affiliation:

[a] Laboratory for Photochemistry and Spectroscopy, Division for Molecular Imaging and Photonics, Department of Chemistry, KU Leuven, Leuven 3001, Belgium.

[b] Department of Biotechnology and Biophysics, Biocenter, University of Würzburg, Am Hubland, 97074 Würzburg, Germany.

[c] Department of Applied Chemistry and Center for Emergent Functional Matter Science, National Yang-Ming Chiao-Tung University, Hsinchu 300093, Taiwan.

[d] AppLightChem, Department of Analytical and Applied Chemistry, Institut Químic de Sarrià, Universitat Ramon Llull, Via Augusta 390, Barcelona 08017, Spain.

[e] Chrometra Scientific B.V., Merelnest 3, 3470 Kortenaken, Belgium.

[f] Max Planck Institute for Polymer Research, 55128 Mainz, Germany.

Abstract:

The self-organization of colloidal nanoparticles into complex structures, both in equilibrium and out-of-equilibrium, is a critical area in colloidal science with potential applications in creating new functional materials. While equilibrium assemblies yield thermodynamically stable and periodic structures, non-equilibrium (or active) assemblies exhibit dynamic, reconfigurable behavior in response to external stimuli. As a consequence, understanding the structure-function relationships in these assemblies remain challenging due to their transient, highly dynamic nature and the limitations of current characterization methods. In this work, we present a novel methodology for Fixation and Resolution of Colloidal Active Matter Ensembles (FRAME). FRAME combines UV photopolymerization to immobilize non-equilibrium (active) colloidal assembly with high-resolution imaging techniques, such as 3D confocal microscopy and SEM, for subsequent structural characterization. We demonstrate this method on Optical Matter (OM) structure formed by an optical trap at glass/water interface where it enables the preservation and detailed analysis of OM structures, using colloidal nanoparticles ranging from 200 nm to 1 μm. We demonstrate the method's efficacy by validating that the immobilization process does not alter the structural properties, allowing for accurate structural analysis. Additionally, this approach enables the capture of dynamic snapshots of the assembly during its formation, providing critical insights into its transient behavior. FRAME offers a new avenue for investigating non-equilibrium colloidal assemblies, paving the way for their rational design and application across a broad range of colloidal systems.

1. Introduction

The self-organization of colloidal nanoparticles (gold, silica, polystyrene…) into intricate and/or periodical structure is a crucial area in colloidal sciences due to their potential to make new functional material.[1,2] Self-assemblies can be broadly classified into equilibrium and out-of-equilibrium types. Equilibrium assemblies form thermodynamically stable, highly periodic structures that can be used in functional materials like colloidal photonic crystals,[3,4] metamaterials[5-7] exhibiting high ($n > 3$) or negative refractive indices,[8-14] and optoelectronic metamaterials based on quantum dot superlattices showing super-fluorescence.[15,16] On the other hand, out-of-equilibrium, or active, self-assemblies respond dynamically to external stimuli (chemical, electrical, optical, magnetic) and offer the advantage of being reconfigurable. In both types of colloidal self-assembly, understanding the interactions between individual components is essential for controlling their spatial arrangement and engineering these materials. Moreover, the relationship between the spatial arrangement, structure and optical properties needs to be unravelled to allow their rational design.[6,17,18]

Due to their dynamic nature, non-equilibrium assemblies of nanoparticles are inherently more challenging to investigate. Their transient behavior requires real-time assembly formation and simultaneous characterization within a single experimental setup, which increases complexity and limits the range of applicable techniques. Additionally, their dynamics restrict the number of methods available, as even optical microscopy struggles with dense, 3D-packed assemblies, making it difficult to distinguish individual particles.[19-21] Therefore, new approaches are needed to study the structure, geometry, and properties of non-equilibrium colloidal assemblies.

As an example of non-equilibrium colloidal assembly, we investigated optical matter (OM). OM is a form of matter in which nanoparticles self-organize through light matter interactions, referred to as optical bonds, resulting in periodical arrangements. These optical bonds originate from multiple scattering interactions between colloidal particles.[19,22-25] As a consequence, OMs can be engineered and reconfigured "on-fly" by modifying the input light properties (wavelength, polarization, intensity profile,…).[26,27] Many examples of optical matter have been created in the literature, such as dumbbell-shaped assemblies in gold particles, chain-like structures in silver particles, and hexagonal clusters in polystyrene particles.[23,29,30] However, detailed information on the structure and/or their properties is often missing, particularly when the density of particle increases, or the size of particle is decreased. However, decreasing the size of particle in OM is crucial as particle smaller than 100 nm are required to use the Rayleigh scattering criteria which ease the comparison between theory and experiment. [28,31] Moreover, metamaterials usually require the size of the nanoparticles to be ~1/5 of the wavelength which yields around (100-200) nm for the visible and NIR light spectrum range.[14] OMs structures are therefore perfect candidates to demonstrate FRAME.

In this study, we developed a novel methodology that combines photo-polymerization reaction to fix non-equilibrium colloidal assemblies into permanent structures, combined with high-resolution imaging for detailed structural analysis. While similar techniques, like photopolymerization,[32-34] optothermal manipulation,[35,36] and light-triggered assembly,[37-42] have succeeded in fixing large

nanoparticles and small clusters, they face limitations in achieving precise large-scale assemblies and struggle with nanoparticles smaller than the diffraction limit during structural analysis. We present a novel workflow, Fixation and Resolution of colloidal Active Matter Ensembles (FRAME), designed to investigate transient/non-equilibrium colloidal assemblies through a two-step process. First, UV photopolymerization is used to lock the non-equilibrium optical matter (OM) assembly within a hydrogel polymer network, which captures the dynamic snapshot of the OM by immobilizing it permanently. Second, high-resolution imaging techniques such as 3D confocal microscopy and SEM are employed to characterize the position and arrangement of the nanoparticles. We applied FRAME to optical matter structures formed via optical trapping at the interface of colloidal nanoparticles ranging from 200 nm to 1 μm. Validation through confocal and SEM imaging confirmed that the workflow does not alter the structural properties of the assemblies. For particles larger than the diffraction limit, FRAME enables 3D structural analysis, including crystallinity and lattice parameters, while high-resolution SEM resolves assemblies with particles below the diffraction limit. This approach facilitates the characterization of non-equilibrium colloidal assemblies, supporting their design for desired applications.

Results and Discussion

2.1 Locking non equilibrium colloidal self-assembly via UV-Photopolymerization

Given the dynamics of non-equilibrium colloidal self-assembly in solution, we need to lock the assembly, to further characterize it. This is the concept of the proposed method FRAME (Fixation and Resolution of colloidal Active Matter Ensembles). The speed of the polymerization process is crucial to ensure that the structure is "instantaneously" locked in place and remains unchanged. Because of this and its high water-solubility, low extinction coefficient and strong UV-absorption at 375 nm, lithium phenyl (2,4,6-trimethylbenzoyl) phosphinate (LAP) was selected as a radical photoinitiator.[43] A UV-365 LED was chosen to maximize UV absorption, and we found that an intensity of 25 mW/cm² was ideal for rapid photopolymerization (Figure S1).

After power optimization, we utilized the LAP as a photoinitiator to synthesize a PAA hydrogel using acrylamide (monomer) and bisacrylamide (crosslinking agent). PAA hydrogel was selected for its inherent hydrophilicity and optical transparency, making it suitable for a wide range of scientific applications.[44] The optical transparency of the hydrogel are functions of the concentrations of monomers, cross-linkers, and the photoinitiator used.[45-47] Hence, the experimental conditions were chosen to ensure rapid photopolymerization (0.2 to 2 seconds) while maintaining a viscosity close to that of water (1-2 cP) to avoid affecting the self-assembly process. The PAA gel was synthesized in a monomer solution containing acrylamide, N,N′-methylenebis(acrylamide) as a crosslinker, and LAP as the photoinitiator. The sample preparation procedure is explained in detail in materials and methods section.

Finally, by adjusting the concentrations of these components and the duration of UV light irradiation, the gel mesh size was optimized to effectively lock smaller nanoparticles in place. We specifically tailored the gel mesh size to match the dimensions of the nanoparticles. To validate this, we conducted single-particle tracking (SPT) experiments using a multiplane widefield microscopy system (Figure S2), which allows for 3D rapid tracking of particle diffusion. The SPT experiments demonstrated that particles with a size equal or larger than 23 nm are effectively

immobilized within the gel mesh network (see Section S3, Supporting Information). To evaluate the FRAME workflow, optical matter (OM) consisting of 1 µm polystyrene microparticles was formed by focusing a 1064 nm laser beam at the glass/solution interface (Figure 1a). Once the OM reached the desired size and arrangement, the UV-LED was turned on to effectively lock the structure in place.

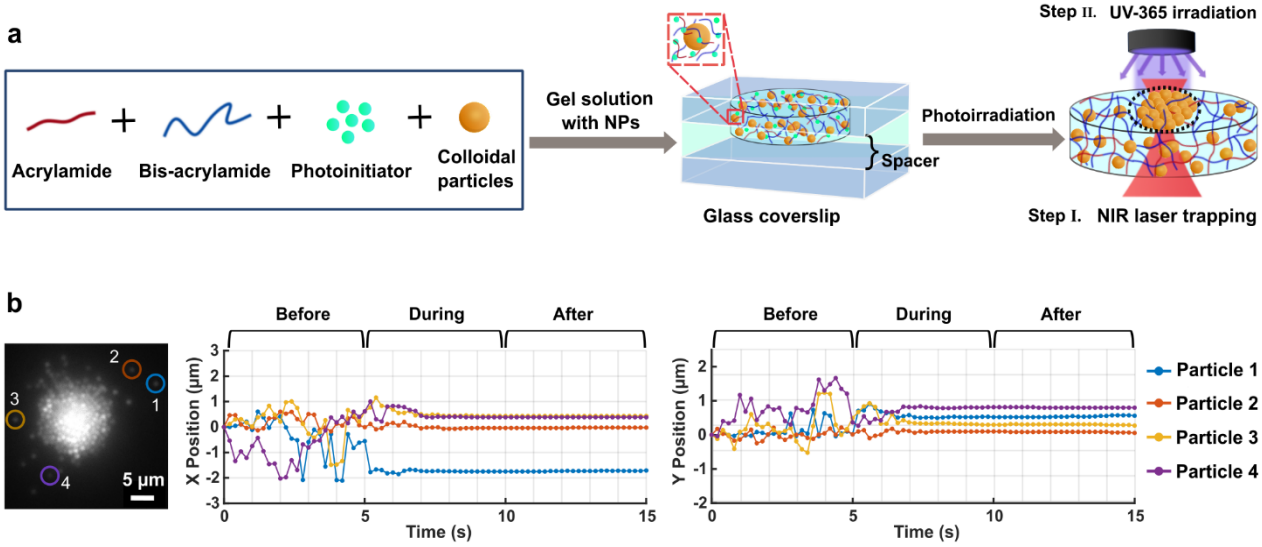

Figure 1. FRAME step 1 - Locking of non-equlibrium optical matter in a photocrosslinked hydrogel. (a) Method illustration: a gel solution containing colloidal particles is placed between two glass coverslips with a spacer, followed by simultaneous irradiation with an NIR trapping laser. Once the optical matter is assembled, and an additional UV light is switched on to lock the optical matter in the hydrogel. (b) Concept validation: a plot showing the X and Y movement of four different particles from the assembly before, during, and after UV irradiation, demonstrating that the particle dynamics are locked in the hydrogel after UV irradiation, based on Single Particle Tracking (SPT) analysis. The positions of four different particles are marked in four different colors corresponding to the plot, and a red circle at the center of the image represents the optical trapping spot.

Single-particle tracking (SPT) experiments were conducted to validate the efficacy of the method. Figure 1b shows the evolution of x and y position of the particles over time. Before UV irradiation, particles inside the optical matter are dynamic but move relatively slow constrained by the surrounding particles, while particle outside (particle 1-4, figure 1b inset) are much more dynamic. Upon UV-365 light irradiation, photopolymerization occurs within 2 seconds, as indicated by the particle traces, which show decreasing fluctuations until they eventually stabilize at zero (Figure 1b). Post UV irradiation, no movement is observed, confirming the formation of permanent optical matter by photopolymerization. The evolution of the dynamic assembly before UV light irradiation into permanent structure after photopolymerization is displayed in Figure S4. The optical matter can then be transported to other characterization tools such as confocal or electron microscope. We note here that while the method was showcased on optical matters, it can be applied to any other type of self-assembly if they can form in the hydrogel solution.

2.2 Validation of FRAME

The second step of FRAME is the high-resolution characterization of the locked, non-equilibrium assembly, in this case, OM. We demonstrate that making the colloidal assembly permanent enables its further structural elucidation using 3D confocal imaging and/or SEM. However, since FRAME involves photopolymerization and post-processing the sample (in case of SEM), we need to ensure that these processes do not affect the created assembly. To achieve this, we utilized 1 µm fluorescent carboxylated polystyrene (PS) microspheres as their size is significantly larger than the diffraction limit of optical microscopy.

For this, the first step of FRAME (Figure 1a) was performed, during which widefield microscopy images were taken before and after gelation, confirming the absence of structural changes. Then, we performed 3D confocal microscopy imaging which successfully resolves the structural properties of the OM in 3D (Figure 2b). Finally, after drying and sputtering with Au/Pd, the sample was imaged using SEM. Note that the SEM imaging was performed in high vacuum condition, which can result the partial drying of the sample,[48] emphasizing the need for checking that the structure remain unchanged throughout. For this, we correlated the confocal images (before SEM sample preparation) and SEM imaging (Figure 2c) of the optical matter.[49] We overlaid the two images and quantified the displacement of microparticles (MPs) in the optical matter between the SEM and confocal images (Figure S5). The average shift of the particles in the X and Y directions was 43 nm and 33 nm, respectively, with some errors attributed to the use of two different imaging systems with distinct environments, magnifications, and other factors.

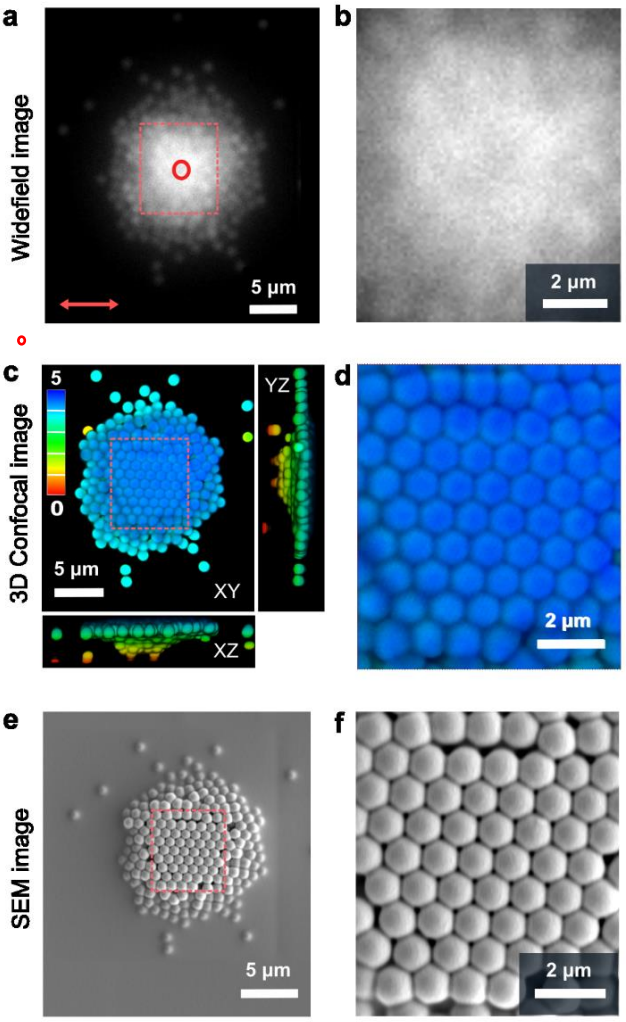

Figure 2. Method validation on fluorescence microparticles (1 µm diameter). The scale bars in (a, c, e) are 5 µm, while in (b, d, f) they are 2 µm. (a) A wide-field microscopy image shows the optical matter of 1 µm PS microparticles, locked after photopolymerization. The red arrow indicates the polarization direction of the 1064 nm NIR trapping laser, and the red circle marks the NIR laser irradiation spot at the center. (c) and (e) depict 3D confocal and scanning electron microscopy (SEM) images, illustrating the embedding of permanent optical matter with PS microparticles in the polymer network. (b, d, f) are magnified views of regions from (a, c, e), respectively.

2.3 3D Structural analysis

After validation of FRAME, we can now use it to characterize our non-equilibrium optical matter system. The 3D confocal microscopy image provides detailed information on the three-dimensional structure of the assemblies which can be extracted via image processing. To achieve this, we developed an approach based on distance matrices (see Materials and Methods). Briefly, the particles are localized in 3D using Gaussian fitting, then, the distances between every possible particle pairs are subsequently calculated in an Euclidean distance matrix. After that, iterating through each layer, we detect triangles that meet specific geometric criteria of common crystal structures (e.g., equilateral triangles with angles close to 60 degrees for hexagonal packing), which can be further analyzed across layers to identify 3D structures like hexagonal prisms. This analysis enables the extraction of the unit lattice and the characterization of the 3D structure of the permanent optical matter (Figure S6). We can also determine the degree of crystallinity of the structure by calculating the ratio of particles that belongs to such unit cells.

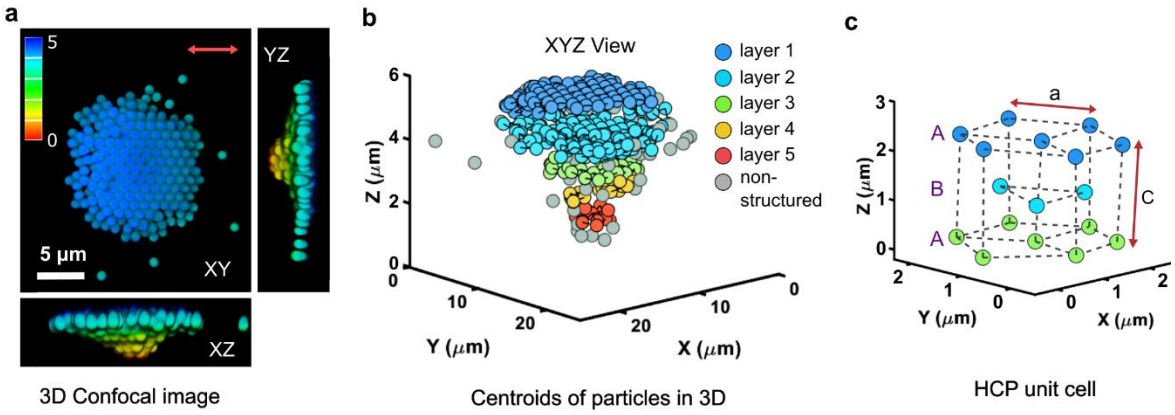

Figure 3. 3D structural analysis of permanent optical matter. (a) 3D confocal microscopy image of the permanent optical matter formed by microparticles locked in a hydrogel. The color bar in the confocal microscopy images indicates the Z-depth arrangement of the particles from top to bottom. (b) Euclidean distance matrix-based analysis used to extract individual layers of particle centroids, revealing specific structural arrangements. The color bar represents the number of particle layers in the assembly from top to bottom. The grey particles in the permanent optical matter are those not forming specific structural arrangements. (c) Hexagonal ABA unit cell extracted from the layer structures, with the lattice parameters and individual layer centroids of the particles represented for the unit cell.

Figure 3 shows an example of OM structure formed, subsequently made permanent using FRAME and then imaged in 3D using a confocal microscope (Figure 3a). Figure 3b shows a graphical representation of the 3D assembly, realized from the 3D localization positions and the known size of the particles where the color code indicates the layer in which the particle belongs. Only the particles that were found to be part of a crystalline structure are colored, representing approximately 80% of the entire assembly. The lattice arrangement follows an ABA packing pattern, with a decrease in particle number from the top surface to the bottom of the assembly. The c/a ratio refers to the ratio of the vertical distance between layers (c) to the horizontal distance between particles (a) in the hexagonal lattice, and it helps describe how the lattice is stacked and spaced in three dimensions. The c/a ratio of the unit lattice was calculated at 1.71 ± 0.15, which is slightly higher than the theoretical lattice constant for hexagonal packing (1.63). However, the

packing efficiency was found to be approximately 71.6%, calculated by averaging the c/a values for the six sides, which is slightly lower than the ideal packing density (74%) of a hcp ABA structure (Figure 3c).

2.4 Controlling particles'arrangement in optical matter structures

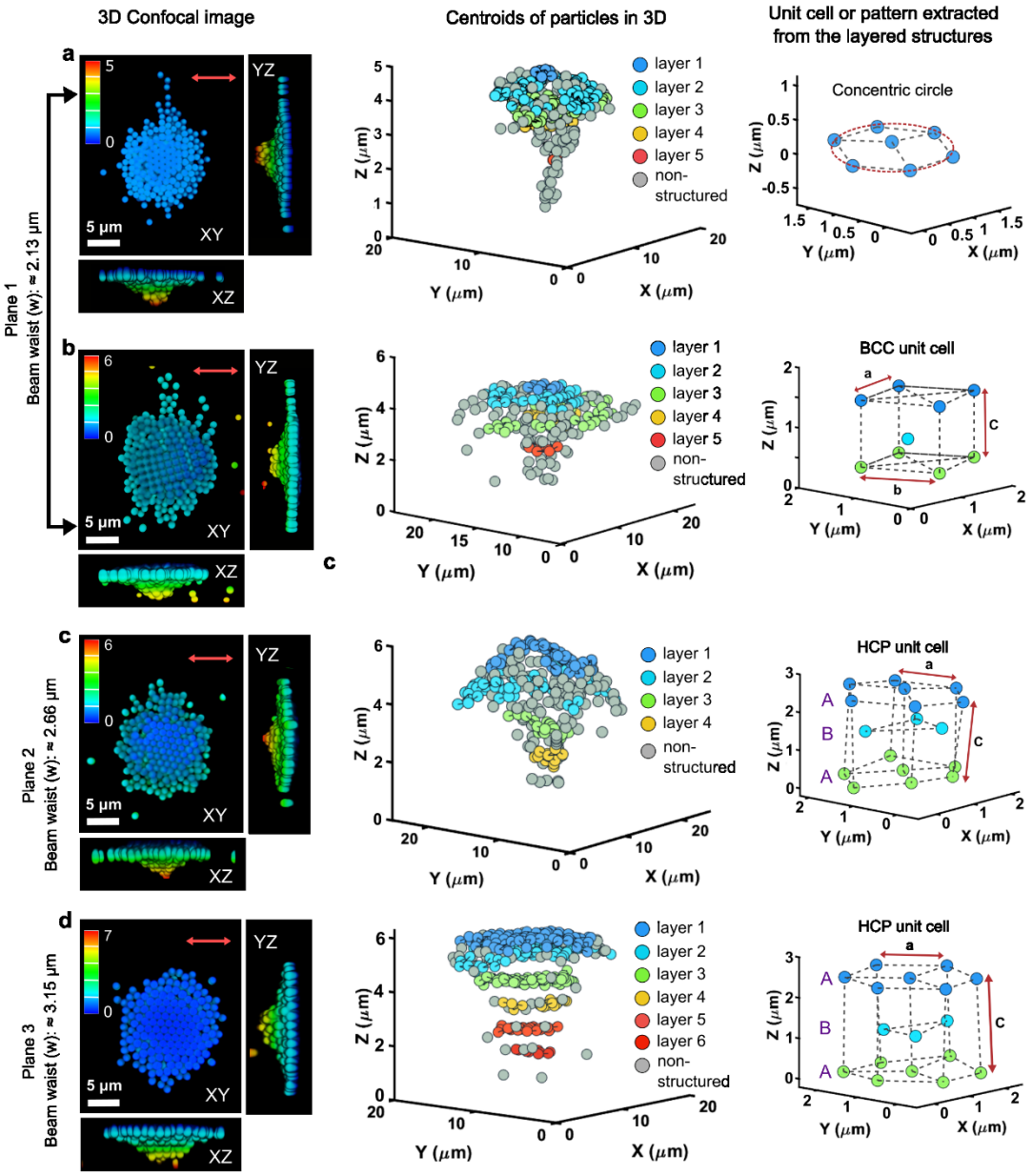

Figure 4. Locking Dynamic Optical Matter Formed at Different Z-Depths. (a, b) 3D confocal microscopy images showing a concentric circle structure, and a BCC (body-centered cubic) lattice unit cell pattern extracted from the layered structures of permanent optical matter, with a beam waist diameter of ~2.13 µm. (c) 3D confocal microscopy image showing an HCP (hexagonal close-packed) ABA lattice obtained at an optical trap with a beam waist diameter of ~2.66 µm. (d) 3D confocal microscopy image showing another HCP ABA lattice obtained at an optical trap with a beam waist diameter of ~3.15 µm. The scale bars for all confocal microscopy images are 5 µm.

Now that we can extract the 3D structure of the non-equilibrium optical matter, it is interesting to see if we can use that feedback to learn how to control the spatial arrangement of the colloidal particles, emphasizing the role of our method in the characterization and design of non-equilibrium colloidal assemblies.

As mentioned earlier, OM structures are formed by the combination of different optical forces. Therefore, for a specific type of particle, the structural arrangement will be mostly dictated by the properties of the light used (wavelength, polarization, power density, area irradiated…). We expect the position of the trapping laser relative to the interface to directly impact the arrangement and crystallinity of the optical matter formed. Henceforth, we used the FRAME to investigate this effect.[50] By focusing the laser at different Z depths (-1.5 µm, -2.5 µm, and -3.5 µm), we were able to study how the relative position of the laser focus to the interface influenced the 3D structure of the optical matter.From the backscattered intensity profile at the focal spot, we determined the beam waist radius (w_0) to be approximately 1.8 µm, with a power density (I_0) of 19.6 MW/cm². The beam waist diameter at Z-depths of -1.5 µm, -2.5 µm, and -3.5 µm was calculated as 2.13 µm, 2.66 µm, and 3.15 µm, respectively, with corresponding power densities of 14 MW/cm², 8.97 MW/cm², and 6.41 MW/cm² (Figure S7). For details, see Section S3.

At a Z-depth of -1.5 µm, corresponding to a higher power density of 14 MW/cm^2, a concentric ring-like structure was observed in approximately 70% of the cases, with most of the particles not contributing to any specific pattern in the optical matter (Figure 4b). In about 30% of the experiments, a cubic-shaped structure appeared at the center of the optical matter, with the cubic lattice parameters being calculated from the observed structure (Figure 4c). At a Z-depth of -2.5 µm, hexagonal packing structures began to form at the center of the optical matter, though fewer particles contributed to the hexagonal arrangement, with the corresponding hexagonal unit cell parameters extracted (Figure 4d). Finally, at a Z-depth of -3.5 µm, the OM exhibited a well-ordered hexagonal packing structure with an ABA pattern, representing the highest packing density observed.

2.5 Locking dynamic optical matter with sub-diffraction limit nanoparticles

One of the factors limiting the characterization of non-equilibrium colloidal assembly such as OM structure is not only their dynamics but also their relatively high packing density which becomes a problem for standard optical microscopy method when the size of the particle's approaches (or are smaller than) the diffraction limit as they cannot be individually resolved. In this section, we demonstrate that our FRAME is also able to characterize optical matter even when formed by particles smaller than the diffraction limit. For this, we used carboxylate-coated fluorescent polystyrene nanoparticles with diameters of 300 nm and 200 nm. After 20 minutes of NIR laser irradiation, a large-scale assembly structure was formed and locked using FRAME methodology. Subsequently, we employed 3D confocal microscopy and SEM imaging to resolve the structure of the resulting permanent optical matter.

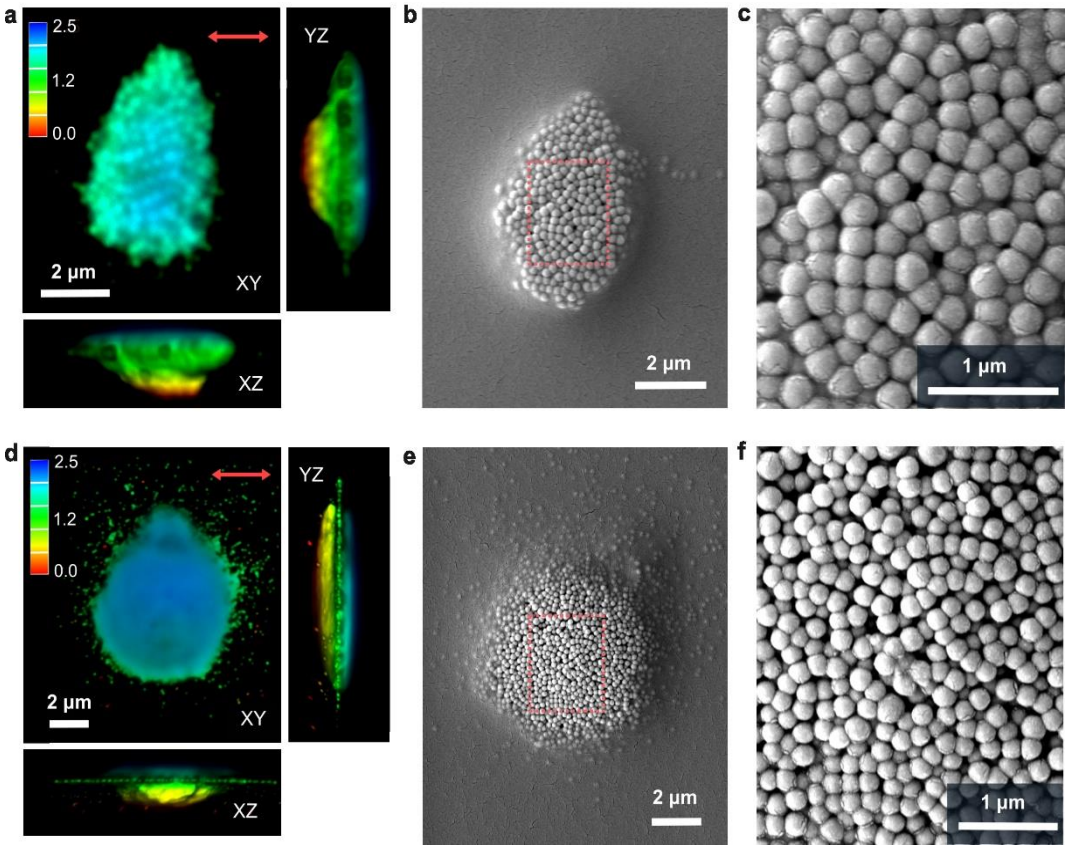

Figure 5. Locking Dynamic Optical Matter Composed of Sub-Diffraction Limit Nanoparticles. (a) 3D confocal microscopy image of 300 nm PS nanoparticles, with the red arrow indicating the polarization direction. (b, c) SEM images showing the assembly of 300 nm PS nanoparticles within the polymer network, with (c) providing a zoomed-in view of the structure. (d) 3D confocal microscopy image of 200 nm PS nanoparticles locked in a hydrogel. (e, f) SEM images displaying the assembly of 200 nm PS nanoparticles within the polymer network, with (f) offering a magnified view of the respective structure. Each scale bar represents 2 μm.

From Figure 5a,d, it can be seen that 3D confocal microscopy struggled to fully resolve the structure, likely due to the size and density issue aforementioned. To overcome this challenge, we utilized high-resolution SEM imaging to investigate the permanent optical matter formed by sub-diffraction limit particles. High-resolution SEM imaging of the optical matter formed by 300 nm PS nanoparticles revealed a close-packed structure with distinct discrete patterns (Figure 5c). We observed random tightly packed arrangement, with small structural units distributed across the assembly. However, For the 200 nm polystyrene particles, a random 3D packing structure was observed, characterized by a highly dense and close-packed order. This arrangement suggests that, despite the randomness in particle placement, the structure achieves a relatively high degree of packing efficiency (Figure 5f). Since the image was captured using SEM, only the surface pattern of the structure can be observed. However, based on the z-depth information obtained from 3D confocal imaging, we estimate that the packing consists of approximately 8 layers of nanoparticles for the 300 nm particles and 12 layers for the 200 nm particles, respectively.

3 Discussion

FRAME, with its rapid photopolymerization and fine mesh size, effectively preserves the structural integrity of non-equilibrium colloidal assemblies. It is important to acknowledge that, given the inherently non-equilibrium nature of these systems, the structure captured by FRAME represents a snapshot of a specific arrangement of the assembly. To fully understand the range of configurations occurring dynamically, multiple samples would need to be immobilized and analysed according to the ergodic hypothesis.REF Despite this, FRAME significantly simplifies the characterization of non-equilibrium self-assemblies using high-resolution imaging techniques. Additionally, because the hydrogel used is fully transparent and has a refractive index similar to that of water (indicate here the refractive index that I calculated in Barcelona vs 1.334, respectively), spectroscopic methods are also applicable. While our focus has been on imaging and structural analysis, this FRAME is versatile and can be integrated with a variety of other characterization techniques.

Our FRAME enables high-resolution structural characterization, providing crucial feedback for controlling structural arrangements and rationally designing materials for specific applications. Using this approach, we discovered that the unit cell and crystallinity of non-equilibrium OM structures can be manipulated by adjusting the laser focus position relative to the assembly's formation site. This adjustment alters the irradiation area and power density, resulting in concentric circle, cubic, or hexagonal crystal structures. These insights could only be obtained with FRAME, making it a key tool for the rational design of non-equilibrium assemblies.

Moreover, our results provide the first detailed structural insight into small nanoparticle assemblies. Although previous studies[20,21,51] indicated the formation of such assemblies, the exact structural details were unclear due to the limitations of optical microscopy and the inability to apply other characterization methods. Our FRAME has revealed that smaller nanoparticles exhibit more chaotic arrangements, lacking clear crystalline patterns. This can be attributed to two factors: smaller particles have higher diffusion coefficients, leading to increased entropy and a greater energy requirement to maintain order. Additionally, the light-matter interactions driving the assembly process, such as multiple scattering, scale with particle volume and these forces are significantly weaker in smaller particles. This challenge has led recent optical matter studies to focus on metallic particles, which have much stronger light-matter interactions due to their plasmonic properties.[31,52,53]

Non-equilibrium colloidal self-assemblies are particularly intriguing because, unlike their equilibrium counterparts, they can be dynamically tuned, reconfigured, and exhibit unique collective behaviors such as flocking, swarming, or propagating waves.[2] These behaviors involve interactions within the colloids and with their surrounding medium, making them ideal, controllable model systems paving the way for intelligent swarming nanorobots.[54] Our FRAME allows for high-resolution characterization of these transient structures and can be integrated with other techniques. By making the assemblies permanent, it also enables the exploitation of their properties for applications, which may not be possible when the structures rapidly change configurations.

4 Conclusion

We demonstrated FRAME, a novel method for locking non-equilibrium colloidal self-assembly via fast photopolymerization. The rate of photopolymerization and the small mesh size ensured that the structure stayed intact as validated by comparing different image modality (optical microscopy, SEM) at different stage of the workflow. By enabling high resolution characterization, our FRAME provides crucial feedback for controlling structural arrangements and rationally designing materials for specific applications. This was demonstrated by forming non-equilibrium optical matter assembly using different beam waist which resulted in different crystalline structures ranging from concentric circle to hexagonal packing. Finally, for the first time we were able to observe the detailed structure of OM structure formed by particles smaller than the diffraction limit demonstrating that their high entropy and weakened light matter interaction made them unable to form a crystalline structure. FRAME enabled crucial insight that would not have been possible by studying these assemblies on their dynamic form. We are convinced that Frame will pave the way for understanding non-equilibrium assembling and enabling their rational design for desired applications.

5 Materials and Methods

4.1 Experimental section

The optical trapping and single particle tracking (SPT) experiments were conducted using a conventional widefield setup. A schematic of the optical setup is illustrated in Figure S2. A 488 nm laser (100 mW, Spectra-Physics) was selected as the widefield excitation source. The widefield excitation laser was focused on the back aperture of an objective lens (NA = 0.90, Olympus UPLFLN 60X Objective) via a widefield lens. The emission light passed through a set of lenses in a 4f configuration and a proprietary prism enabling multiplane imaging. The different imaging planes were collected by two sCMOS cameras, with four image planes each. For the optical trapping experiment, the NIR laser 1064 nm (Laser Quantum Opus 1064, UK) was used. The 1064 nm laser was focused at the same back aperture of the objective lens by passing through a beam expander and mirrors.

The 3D confocal microscopy measurements were performed using a Leica SP8 confocal microscopy setup (TCS SP8 multiphoton system). The 3D Z-stack imaging was conducted using a 100X oil objective (HC PL APO 100x/1.40-0.70 OIL) and hybrid detectors. The white light laser (WLL) was selected as the excitation source with an excitation wavelength of 488 nm. The Z-stack scan was performed with a line average of 3, an image acquisition speed of 100, and a Z-depth of 100 nm. The electron microscopy experiment was performed with a JSM-7200F field scanning electron microscope.

4.2 Sample preparation

The carboxylate-coated polystyrene latex beads were purchased from ThermoFisher Scientific (Carboxylate-Labeled Microspheres, 0.2 μm, yellow-green fluorescent 505/515, 1% solids). The gel solution was prepared with 12.5 wt% of acrylamide (≥ 99%, Sigma Aldrich, Germany), 0.3 wt% of N,N'-methylenebisacrylamide (≥ 99.5%, Sigma Aldrich, Germany), 0.44 wt% of lithium phenyl-2,4,6-trimethylbenzoylphosphinate photoinitiator (≥ 95%, Sigma Aldrich, Germany), and MQ water. The coverslip was cleaned using UV-ozone treatment for 60 minutes to clean the glass surface. The top coverslip was made hydrophobic using a saline Sigmacote, purchased from Sigma Aldrich, Germany. The gel solution containing nanoparticles was placed within a glass coverslip using imaging spacers. The 0.12 mm thickness with 20 mm well diameter double-sided imaging spacers (Grace Bio-Labs SecureSeal™ imaging spacer) were used for sample preparation. During gelation, a saline Sigmacote-coated coverslip was putted on the top of the sample. After gelation occurred, the top coverslip was carefully removed from the hydrogel due to its hydrophobic properties, and 3D confocal imaging was then acquired as follow. The sample was air-dried for 3 hours and then sputtered with Au/Pd for 60 s (JEOL JFC-1300, Automatic Sputter Coater) prior to the scanning electron microscopy (SEM) imaging. The electron microscopy imaging was performed by using a high-resolution SEM (JSM-7200F field electron SEM).

4.3 Confocal/SEM correlation

Segmentation analysis was performed on the SEM images (Figure S5), and the centroids (Cx, Cy) were mathematically calculated based on the center of mass of the pixels constituting the particles (see Section S5, Supporting Information). The centroid of the confocal microscopy image was

determined by 2D Gaussian fittings. The centroids from the confocal and SEM images were overlaid to calculate the particle shift observed in SEM relative to confocal imaging.

4.4 Euclidian based structural analysis

The centroid of each particle was obtained through 3D Gaussian fitting of the confocal microscopy images. To analyze the 3D structure of the optical matter and extract specific structural arrangements, such as the hexagonal close-packed (HCP) lattice, Euclidean distance-based calculations were essential. The process began with the preparation of the particle position data, where the 3D coordinates (x, y, z) of the particles were loaded into a matrix. This data was initially in pixel units, so a conversion factor was applied to transform these values into physical units, such as micrometers. Next, the particles were segmented into distinct layers based on their Z-coordinates (Figure 3b). This was achieved by defining a specific layer thickness, with particles within a certain Z-range grouped into the same layer. A Z-error margin of 20-30% was also considered to account for minor variations in the Z-coordinate, ensuring that particles within a specific range were correctly identified as part of the same layer.

Once the layers are defined, a Euclidean distance matrix is computed for each layer. This matrix contains the distances between every pair of particles within the layer, calculated using Eq. 1:

$$d_{ij} = \sqrt{\left(x_i - x_j\right)^2 + \left(y_i - y_j\right)^2}$$

Where d_{ij} is the distance between particles i and j *and* x and y are their respective coordinates. This calculation is crucial for identifying equilateral triangles formed by neighboring particles, which are indicative of hexagonal packing.

References:

[1] Boles, M. A.; Engel, M.; Talapin, D. V. Self-Assembly of Colloidal Nanocrystals: From Intricate Structures to Functional Materials. *Chem. Rev.* **2016**, *116*, 11220−11289.

[2] Huang, Y.; Wu, C.; Chen, J.; Tang, J. Colloidal Self-Assembly: From Passive to Active Systems. *Angew. Chem. Int. Ed.* **2024**, *63*, e202313885.

[3] Hynninen, A.-P.; Thijssen, J. H. J.; Vermolen, E. C. M.; Dijkstra, M.; van Blaaderen, A. Self-Assembly Route for Photonic Crystals with a Bandgap in the Visible Region. *Nat. Mater.* **2007**, *6*, 202−205.

[4] Cai, Z.; Li, Z.; Ravaine, S.; He, M.; Song, Y.; Yin, Y.; Zheng, H.; Teng, J.; Zhang, A. From Colloidal Particles to Photonic Crystals: Advances in Self-Assembly and Their Emerging Applications. *Chem. Soc. Rev.* **2021**, *50*, 5898−5951.

[5] Bian, T.; Gardin, A.; Gemen, J.; Houben, L.; Perego, C.; Lee, B.; Elad, N.; Chu, Z.; Pavan, G. M.; Klajn, R. Electrostatic Co-Assembly of Nanoparticles with Oppositely Charged Small Molecules into Static and Dynamic Superstructures. *Nat. Chem.* **2021**, *13*, 940−949.

[6] Chen, S.; Parker, J. A.; Peterson, C. W.; Rice, S. A.; Scherer, N. F.; Ferguson, A. L. Understanding and Design of Non-Conservative Optical Matter Systems Using Markov State Models. *Mol. Syst. Des. Eng.* **2022**, *7*, 1228−1238.

[7] Liang, L.; Wu, L.; Zheng, P.; Ding, T.; Ray, K.; Barman, I. DNA-Patched Nanoparticles for the Self-Assembly of Colloidal Metamaterials. *JACS Au* **2023**, *3*, 1176−1184.

[8] Kim, J. Y.; Kim, H.; Kim, B. H.; Chang, T.; Lim, J.; Jin, H. M.; Mun, J. H.; Choi, Y. J.; Chung, K.; Shin, J.; Fan, S.; Kim, S. O. Highly Tunable Refractive Index Visible-Light Metasurface from Block Copolymer Self-Assembly. *Nat. Commun.* **2016**, *7*, 12911.

[9] Colloidal Superlattices for Unnaturally High-Index Metamaterials at Broadband Optical Frequencies. Opt. Express 2015, 23, 28170−28181.

[10] Colloidal Superlattices for Unnaturally High-Index Metamaterials at Broadband Optical Frequencies. *Langmuir* **2013**, *29*, 1551−1561.

[11] Malassis, L.; Massé, P.; Tréguer-Delapierre, M.; Mornet, S.; Weisbecker, P.; Barois, P.; Simovski, C. R.; Kravets, V. G.; Grigorenko, A. N. Topological Darkness in Self-Assembled Plasmonic Metamaterials. *Adv. Mater.* **2014**, *26*, 324−330.

[12] Shafiei, F.; Monticone, F.; Le, K. Q.; Liu, X. X.; Hartsfield, T.; Alù, A.; Li, X. A Subwavelength Plasmonic Metamolecule Exhibiting Magnetic-Based Optical Fano Resonance. *Nat. Nanotechnol.* **2013**, *8*, 95−99.

[13] Shalaev, V. M. Optical Negative-Index Metamaterials. *Nat. Photonics* **2007**, *1*, 41−48.

[14] Huh, J.-H.; Kim, K.; Im, E.; Lee, J.; Cho, Y.; Lee, S. Exploiting Colloidal Metamaterials for Achieving Unnatural Optical Refractions. *Adv. Mater.* **2020**, *32*, 2001806.

[15] Rainò, G.; Becker, M. A.; Bodnarchuk, M. I.; Mahrt, R. F.; Kovalenko, M. V.; Stöferle, T. Superfluorescence from Lead Halide Perovskite Quantum Dot Superlattices. *Nature* **2018**, *563*, 671−675.

[16] Pinna, J.; Pili, E.; Mehrabi Koushki, R.; Gavhane, D. S.; Carlà, F.; Kooi, B. J.; Portale, G.; Loi, M. A. PbI_2 Passivation of Three-Dimensional PbS Quantum Dot Superlattices Toward Optoelectronic Metamaterials. *ACS Nano* **2024**, *18*, 19124−19136.

[17] Kadic, M.; Milton, G. W.; van Hecke, M.; Wegener, M. 3D Metamaterials. *Nat. Rev. Phys.* **2019**, *1*, 201−214.

[18] Wang, K.; Park, S. H.; Zhu, J.; Kim, J. K.; Zhang, L.; Yi, G.-R. Self-Assembled Colloidal Nanopatterns Toward Unnatural Optical Meta-Materials. *Adv. Funct. Mater.* **2021**, *31*, 2008246.

[19] Huang, C.-H.; Louis, B.; Bresoli-Obach, R.; Kudo, T.; Camacho, R.; Scheblykin, I. G.; Sugiyama, T.; Hofkens, J.; Masuhara, H. The Primeval Optical Evolving Matter by Optical Binding Inside and Outside the Photon Beam. *Nat. Commun.* **2022**, *13*, 5325.

[20] Wang, S.-F.; Yuyama, K.; Sugiyama, T.; Masuhara, H. Reflection Microspectroscopic Study of Laser Trapping Assembling of Polystyrene Nanoparticles at Air/Solution Interface. *J. Phys. Chem. C* **2016**, *120*, 15578−15585.

[21] Kudo, T.; Wang, S.-F.; Yuyama, K.; Masuhara, H. Optical Trapping-Formed Colloidal Assembly with Horns Extended to the Outside of a Focus Through Light Propagation. *Nano Lett.* **2016**, *16*, 3058−3062.

[22] Wei, M.-T.; Ng, J.; Chan, C. T.; Ou-Yang, H. D. Lateral Optical Binding Between Two Colloidal Particles. *Sci. Rep.* **2016**, *6*, 38883.

[23] Huang, C.-H.; Louis, B.; Rocha, S.; Liz-Marzán, L. M.; Masuhara, H.; Hofkens, J.; Bresolí-Obach, R. Plasmonic Dipole and Quadrupole Scattering Modes Determine Optical Trapping, Optical Binding, and Swarming of Gold Nanoparticles. *J. Phys. Chem. C* **2024**, *128*, 5731–5740.

[24] Dholakia, K.; Zemánek, P. Colloquium: Gripped by Light: Optical Binding. *Rev. Mod. Phys.* **2010**, *82*, 1767−1791.

[25] Zhang, C.; Muñetón Díaz, J.; Muster, A.; Abujetas, D. R.; Froufe-Pérez, L. S.; Scheffold, F. Determining Intrinsic Potentials and Validating Optical Binding Forces Between Colloidal Particles Using Optical Tweezers. *Nat. Commun.* **2024**, *15*, 1020.

[26] Shoji, T.; Tamura, M.; Kameyama, T.; Iida, T.; Tsuboi, Y.; Torimoto, T. Nanotraffic Lights: Rayleigh Scattering Microspectroscopy of Optically Trapped Octahedral Gold Nanoparticles. *J. Phys. Chem. C* **2019**, *123*, 23096−23102.

[27] Maragò, O. M.; Jones, P. H.; Gucciardi, P. G.; Volpe, G.; Ferrari, A. C. Optical Trapping and Manipulation of Nanostructures. *Nat. Nanotechnol.* **2013**, *8*, 807−819.

[28] Masuhara, H.; Yuyama, K.-I. Optical Force-Induced Chemistry at Solution Surfaces. *Annu. Rev. Phys. Chem.* **2021**, *72*, 565−589.

[29] Pradhan, S.; Whitby, C. P.; Williams, M. A. K.; Chen, J. L. Y.; Avci, E. Surface Interaction and Stability of Emulsions: Insights into the Role of Droplet Size and Wettability. *J. Colloid Interface Sci.* **2022**, *621*, 101-109.

[30] Yan, Z.; Shah, R. A.; Chado, G.; Gray, S. K.; Pelton, M.; Scherer, N. F. Guiding Spatial Arrangements of Silver Nanoparticles by Optical Binding Interactions in Shaped Light Fields. *ACS Nano* **2013**, *7*, 1790–1802.

[31] Forbes, K. A.; Bradshaw, D. S.; Andrews, D. L. Optical Binding of Nanoparticles. *Nanophotonics* **2020**, *9*, 361.

[32] Chen, Z.; Nan, F.; Yan, Z. Making Permanent Optical Matter of Plasmonic Nanoparticles by In Situ Photopolymerization. *J. Phys. Chem. C* **2020**, *124*, 4215−4220.

[33] Jiménez Amaya, A.; Goldmann, C.; Hill, E. H. Thermophoresis-Induced Polymer-Driven Destabilization of Gold Nanoparticles for Optically Directed Assembly at Interfaces. *Small Methods* **2024**, 2400828.

[34] Peng, X. L.; Li, J. G.; Lin, L. H.; Liu, Y. R.; Zheng, Y. B. Opto-Thermophoretic Manipulation and Construction of Colloidal Superstructures in Photocurable Hydrogels. *ACS Appl. Nano Mater.* **2018**, *1*, 3998−4004.

[35] Kollipara, P. S.; Wu, Z.; Yao, K.; Lin, D.; Ju, Z.; Zhang, X.; Jiang, T.; Ding, H.; Fang, J.; Li, J.; Korgel, B. A.; Redwing, J. M.; Yu, G.; Zheng, Y. Three-Dimensional Optothermal Manipulation of Light-Absorbing Particles in Phase-Change Gel Media. *ACS Nano* **2024**, *18*, 8062−8072.

[36] Li, J.; Zheng, Y. Optothermally Assembled Nanostructures. *Acc. Mater. Res.* **2021**, *2*, 352–363.

[37] De Fazio, A. F.; El-Sagheer, A. H.; Kahn, J. S.; Nandhakumar, I.; Burton, M. R.; Brown, T.; Muskens, O. L.; Gang, O.; Kanaras, A. G. Light-Induced Reversible DNA Ligation of Gold Nanoparticle Superlattices. *ACS Nano* **2019**, *13*, 5771−5777.

[38] Wang, J.; Peled, T. S.; Klajn, R. Photocleavable Anionic Glues for Light-Responsive Nanoparticle Aggregates. *J. Am. Chem. Soc.* **2023**, *145*, 4098−4108.

[39] Melzer, J. E.; McLeod, E. Assembly of Multicomponent Structures from Hundreds of Micron-Scale Building Blocks Using Optical Tweezers. *Microsyst. Nanoeng.* **2021**, *7*, 45.

[40] Chizari, S.; Lim, M. P.; Shaw, L. A.; Austin, S. P.; Hopkins, J. B. Automated Optical-Tweezers Assembly of Engineered Microgranular Crystals. *Small* **2020**, *16*, e2000314.

[41] Gonzalez-Garcia, M. C.; Garcia-Fernandez, E.; Hueso, J. L.; Paulo, P. M. R.; Orte, A. Optical Binding-Driven Micropatterning and Photosculpting with Silver Nanorods. *Small Methods* **2023**, *7*, 2300076.

[42] Gao, D.; Ding, W.; Nieto-Vesperinas, M.; Ding, X.; Rahman, M.; Zhang, T.; Lim, C. T.; Qiu, C.-W. Optical Manipulation from the Microscale to the Nanoscale: Fundamentals, Advances and Prospects. *Light Sci. Appl.* **2007**, *6*, e17039.

[43] Fairbanks, B. D.; Schwartz, M. P.; Bowman, C. N.; Anseth, K. S. Photoinitiated Polymerization of PEG-Diacrylate with Lithium Phenyl-2,4,6-Trimethylbenzoylphosphinate: Polymerization Rate and Cytocompatibility. *Biomaterials* **2009**, *30*, 6702−6707.

[44] Chan, D.; Chien, J.-C.; Axpe, E.; Blankemeier, L.; Baker, S. W.; Swaminathan, S.; Piunova, V. A.; Zubarev, D. Y.; Maikawa, C. L.; Grosskopf, A. K.; Mann, J. L.; Soh, H. T.; Appel, E. A. Combinatorial Polyacrylamide Hydrogels for Preventing Biofouling on Implantable Biosensors. *Adv. Mater.* **2022**, *34*, 2109764.

[45] Tse, J. R.; Engler, A. J. Preparation of Hydrogel Substrates with Tunable Mechanical Properties. *Curr. Protoc. Cell Biol.* **2010**, *47*, 10.16.1−10.16.16.

[46] Wang, Y.; Nian, G.; Kim, J.; Suo, Z. Polyacrylamide Hydrogels. VI. Synthesis-Property Relation. *J. Mech. Phys. Solids* **2023**, *170*, 105099.

[47] Sheth, S.; Jain, E.; Karadaghy, A.; Syed, S.; Stevenson, H.; Zustiak, S. P. UV Dose Governs UV-Polymerized Polyacrylamide Hydrogel Modulus. *Int. J. Polym. Sci.* **2017**, 5147482.

[48] Arenas Esteban, D.; Wang, D.; Kadu, A.; Olluyn, N.; Sánchez-Iglesias, A.; Gomez-Perez, A.; González-Casablanca, J.; Nicolopoulos, S.; Liz-Marzán, L. M.; Bals, S. Quantitative 3D Structural Analysis of Small Colloidal Assemblies Under Native Conditions by Liquid-Cell Fast Electron Tomography. *Nat. Commun.* **2024**, *15*, 6399.

[49] Ando, T.; Bhamidimarri, S. P.; Brending, N.; Colin-York, H.; Collinson, L.; De Jonge, N.; De Pablo, P. J.; Debroye, E.; Eggeling, C.; Franck, C.; Fritzsche, M.; Gerritsen, H.; Giepmans, B. N. G.; Grunewald, K.; Hofkens, J.; Hoogenboom, J. P.; Janssen, K. P. F.; Kaufmann, R.; Klumperman, J.; Kurniawan, N.; Kusch, J.; Liv, N.; Parekh, V.; Peckys, D. B.; Rehfeldt, F.; Reutens, D. C.; Roeffaers, M. B. J.; Salditt, T.; Schaap, I. A. T.; Schwarz, U. S.; Verkade, P.; Vogel, M. W.; Wagner, R.; Winterhalter, M.; Yuan, Y.; Zifarelli, G. The 2018 Correlative Microscopy Techniques Roadmap. *J. Phys. D: Appl. Phys.* **2018**, *51*, 443001.

[50] Louis, B.; Camacho, R.; Bresolí-Obach, R.; Abakumov, S.; Vandaele, J.; Kudo, T.; Masuhara, H.; Scheblykin, I. G.; Hofkens, J.; Rocha, S. Fast-Tracking of Single Emitters in Large Volumes with Nanometer Precision. *Opt. Express* **2020**, *28*, 28656−28671.

[51] Lu, J.-S.; Kudo, T.; Louis, B.; Bresolí-Obach, R.; Scheblykin, I. G.; Hofkens, J.; Masuhara, H. Optical Force-Induced Dynamics of Assembling, Rearrangement, and Three-Dimensional Pistol-like Ejection of Microparticles at the Solution Surface. *J. Phys. Chem. C* **2020**, *124*, 27107−27117.

[52] Svedberg, F.; Li, Z.; Xu, H.; Käll, M. Creating Hot Nanoparticle Pairs for Surface-Enhanced Raman Spectroscopy through Optical Manipulation. *Nano Lett.* **2006**, *6*, 2639−2641.

[53] Demergis, V.; Florin, E. L. Ultrastrong Optical Binding of Metallic Nanoparticles. *Nano Lett.* **2012**, *12*, 5756−5760.

[54] Liu, A. T.; Hempel, M.; Yang, J. F.; Brooks, A. M.; Pervan, A.; Koman, V. B.; Zhang, G.; Kozawa, D.; Yang, S.; Goldman, D. I.; Miskin, M. Z.; Richa, A. W.; Randall, D.; Murphey, T. D.; Palacios, T.; Strano, M. S. Colloidal Robotics. *Nat. Mater.* **2023**, *22*, 1453–1462.